JOURNAL OF GEOPHYSICAL RESEARCH: SPACE PHYSICS, VOL. 119, 431–440, doi:10.1002/2013JA019247, 2014

Modeling ionospheric disturbance features in quasi-vertically incident ionograms using 3-D magnetoionic ray tracing and atmospheric gravity waves

M. A. Cervera[1] and T. J. Harris[1]

Received 24 July 2013; revised 3 December 2013; accepted 4 December 2013; published 8 January 2014.

[1] The Defence Science and Technology Organisation (DSTO) has initiated an experimental program, Spatial Ionospheric Correlation Experiment, utilizing state-of-the-art DSTO-designed high frequency digital receivers. This program seeks to understand ionospheric disturbances at scales < 150 km and temporal resolutions under 1 min through the simultaneous observation and recording of multiple quasi-vertical ionograms (QVI) with closely spaced ionospheric control points. A detailed description of and results from the first campaign conducted in February 2008 were presented by Harris et al. (2012). In this paper we employ a 3-D magnetoionic Hamiltonian ray tracing engine, developed by DSTO, to (1) model the various disturbance features observed on both the *O* and *X* polarization modes in our QVI data and (2) understand how they are produced. The ionospheric disturbances which produce the observed features were modeled by perturbing the ionosphere with atmospheric gravity waves.

Citation: Cervera, M. A., and T. J. Harris (2014), Modeling ionospheric disturbance features in quasi-vertically incident ionograms using 3-D magnetoionic ray tracing and atmospheric gravity waves, *J. Geophys. Res. Space Physics*, *119*, 431–440, doi:10.1002/2013JA019247.

1. Introduction

1.1. HF Ray Tracing Techniques

[2] Hamilton's variational principle is a powerful technique for studying physical systems where the principle of stationary action (dynamical systems) or Fermat's principle of stationary time (ray propagation) applies. *Haselgrove* [1955] set down the Hamiltonian (or canonical) equations of the raypath of HF radio waves propagating in the Earth's ionosphere. The effect of the Earth's magnetic field was included and so separate raypaths for the ordinary (*O*) and extraordinary (*X*) polarization modes could be obtained. The canonical equations for the raypath are not able to be solved analytically for a general ionosphere and so *Haselgrove and Haselgrove* [1960] and *Haselgrove* [1963] reformulated the equations, apropos finding a solution via numerical integration techniques. The canonical equations, now commonly known as Haselgrove's equations, have been used extensively over many years to study HF radio wave propagation [e.g., *Croft*, 1967; *Surtees*, 1968a; *Bennett*, 1969, 1973; *Jones and Stephenson*, 1975; *Nickisch*, 1988; *Reilly*, 1991; *Västberg and Lundborg*, 1996; *Strangeways*, 2000; *Tsai et al.*, 2010]. In most cases the equations were recast in spherical coordinates (Haselgrove used the Cartesian coordinate system).

[3] Due to the high computational overheads of numerical ray tracing (NRT) for the full 3-D magnetoionic case, many researchers developed simplified formulations for their studies. These include analytical ray tracing (ART) [*Croft and Hoogasian*, 1968; *Dyson and Bennett*, 1988; *Norman et al.*, 1997], 2-D numerical ray tracing [*Coleman*, 1997, 1998], and 3-D ray tracing where the effect of the Earth's magnetic field is ignored [*Paul et al.*, 1968; *Helms and Thompson*, 1973] (*Russell et al.* [1997], based on Bennett's work). All of these techniques require compromises to be made, e.g., ART ignores the effect of the Earth's magnetic field and assumes a spherical ionosphere whose profile is described by quasi-parabolic [*Croft and Hoogasian*, 1968] or quasi-cubic [*Norman et al.*, 1997] segments. Coleman's 2-D NRT allows for a general ionospheric profile which varies downrange, but ray propagation is confined to a plane and again the effect of the Earth's magnetic field is ignored. None of these techniques is able to separately calculate the raypaths of the *O* and *X* polarization modes. *Bennett et al.* [2004] provide a recent comprehensive review of the various HF ray tracing techniques.

[4] Recently, *Coleman* [2011] developed a unique point-to-point ray tracing method. Coleman's alternative approach is to directly solve the variational principle so that all the points which define the raypath are determined simultaneously. However, for this technique to work, an initial estimate of the raypath is required which is supplied by a

Additional supporting information may be found in the online version of this article.

[1]Defence Science and Technology Organisation, Edinburgh, South Australia, Australia.

Corresponding author: M. A. Cervera, Defence Science and Technology Organisation, West Ave., PO Box 1500, Edinburgh, SA 5111, Australia. (manuel.cervera@dsto.defence.gov.au)

2169-9380/14/10.1002/2013JA019247

simpler technique (ray homing using ART or 2-D NRT). The advantage of Coleman's technique is that computationally intensive ray homing using 3-D magnetoionic ray tracing is no longer required to determine the point-to-point raypath.

[5] Later in this paper we use the "traditional" method of 3-D magnetoionic ray tracing based on Haselgrove's equations (see section 2). While Coleman's method is appropriate for oblique paths, obtaining an initial estimate of the raypath for the near-vertical case of our experimental setup is not possible (see section 3.2).

1.2. Ray Trace Modeling of Ionospheric Disturbances

[6] Ionospheric disturbances have long been known to cause additional cusps, loops, and other disturbance features on the traces of HF soundings of the ionosphere [e.g., *Munro*, 1953]. From the consideration of the reflection of oblique echoes from traveling ionospheric disturbances (TIDs), *Munro* [1953] and *Munro and Heisler* [1956a] explained how these additional cusps and loops could manifest on ionograms [see also *Booker*, 1961]. Furthermore, *Munro and Heisler* [1956a] demonstrated that the uplift in the isoionic contours caused by the passage of the TID is also displaced horizontally with height, in the direction of motion of the TID. Later, *Munro and Heisler* [1956b] explained that the divergence of the *O* and *X* polarization modes in the ionosphere is the reason for the manifestation of the TID on the *X*-mode trace occurring later than on the *O*-mode trace.

[7] The early work of *Munro* [1953] and *Munro and Heisler* [1956a] did not employ ray tracing, and while it was carefully thought out and developed, it was ultimately qualitative in nature. *Paul et al.* [1968] were amongst the first researchers to apply ray tracing techniques to the modeling of a disturbance observed in a vertically incident ionogram. The disturbance modeled was artificially produced by a chemical release from a rocket, which we note is likely to be different to that produced by a TID. However, due to the computational overheads, their work was limited to a case study of a single ionogram and the effect of the Earth's magnetic field was ignored. *Surtees* [1968a, 1968b] modeled the effect of naturally occurring TIDs for the case of oblique propagation using a 3-D NRT computer program developed by *Jones* [1968]; magnetic field effects were not modeled.

[8] *Helms and Thompson* [1973] modeled TIDs as large "Gaussian" depletions, or troughs, in electron density, phase advanced with height (i.e., tilted) in the direction of travel. They used 3-D NRT to synthesize disturbed vertically incident ionograms. However, as with *Paul et al.* [1968], the effect of the Earth's magnetic field was not included and the number of simulations was limited. Only three ionograms were synthesized; in each case the TID was set in a different location with respect to the sounder.

[9] To gain better insight from a modeling perspective, of how TIDs affect ionograms, *Lobb and Titheridge* [1977] employed 2-D ART to synthesize the disturbed ionograms. The reduced computational load of their ART-based model allowed *Lobb and Titheridge* to generate many synthetic ionograms and so they were able to investigate the time evolution of the modeled disturbed ionogram as they moved the TIDs through the field of view of the sounder. The Gaussian trough model of TIDs introduced by *Helms and Thompson* [1973] was used for their work along with a variation viz, Gaussian enhancements in the background ionosphere.

[10] *Kalikhman et al.* [1992] used 3-D NRT to model the effect of the growth of an artificially induced ionospheric hole on ionograms. However, while they used a full magnetoionic 3-D NRT, they simplified their calculations by limiting their model to the particular case of *O*-mode propagation where the wave normal, magnetic field vector, and electron density gradient were coplanar. The raypaths, for this case, do not undergo any out-of-plane deviations; all rays lie in the same plane. The *X*-mode case was not modeled at all.

[11] More recently, the synthesis of TID signatures observed by the CUTLASS HF radar has been carried out by *Stocker et al.* [2000]. They used a modified version of the 3-D NRT code of *Jones and Stephenson* [1975] where the effects of the magnetic field were ignored (the *Jones and Stephenson* code normally accounts for the magnetic field).

[12] Modern computers allow us to make use of computationally intensive 3-D magnetoionic ray tracing to synthesize both the *O* and *X* traces of disturbed ionograms at a temporal resolution that is high enough to allow *movies* of the disturbed ionograms to be produced that illustrate passage of a TID. We describe in this paper how the movies are produced and compare them directly with the 1 min resolution Spatial Ionospheric Correlation Experiment (SpICE) movies of the TIDs observed by *Harris et al.* [2012]. We also investigate the different effects that the TIDs often exhibit on the *O* and *X* polarization modes.

2. PHaRLAP

[13] The Defence Science and Technology Organisation (DSTO) has developed a HF radio wave ray tracing toolbox (PHaRLAP) in order to study the propagation of radio waves through the ionosphere. PHaRLAP provides a variety of ray tracing engines of various sophistication from 2-D ray tracing to full 3-D magnetoionic ray tracing. The 2-D raytracing engine is an implementation of the 2-D equations developed by *Coleman* [1997, 1998], while the 3-D engine is based upon the equations of *Haselgrove* [1963].

[14] Many previous researchers have used the *Jones and Stephenson* [1975] 3-D raytracing code for their raypath calculations. This code implements the Haselgrove equations in spherical coordinates due to the spherical geometry of the Earth and the ionosphere. However, *Haselgrove* [1963] opines that the simplicity of the Cartesian form outweighs the extra complication of expressing a spherical ionospheric layer in these terms.

[15] We followed *Haselgrove* [1963] and implemented the equations in her original Cartesian form. Irrespective of previous arguments about this being the simpler form to implement, the Cartesian form has the advantage that it is easier to convert the solution for the raypath to World Geodetic System 1984 (WGS84) coordinates. WGS84 is the reference coordinate system used by the Global Positioning System (GPS) [*EL-Rabbany*, 2006]. The gridded ionosphere and geomagnetic field supplied to the algorithm are also specified in WGS84 coordinates. Precise routines for the transformation of Cartesian to WGS84 coordinates require iterative techniques and are therefore slow. This is not acceptable for our purposes as the transformation takes place at the heart of the numerical integration. The transform is required to be fast and so we use an approximate

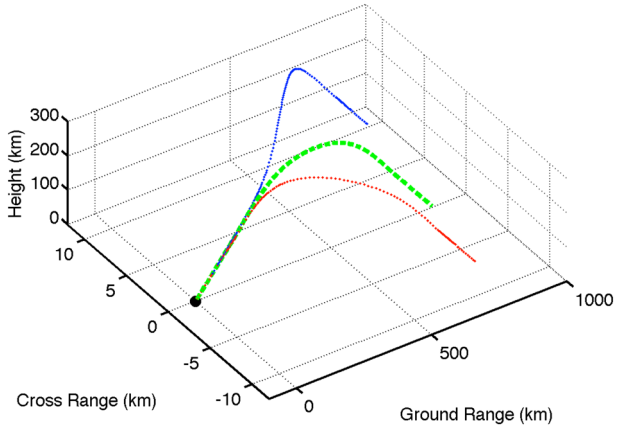

Figure 1. Example of 3-D ray tracing with PHaRLAP showing *O* (blue) and *X* (red) polarization modes and the case for no geomagnetic field (green).

noniterative method based upon the geocentric to geodetic latitude coordinate conversion algorithm of *Mathworks* [2013] which we found to have acceptable precision close to the Earth (the solution has no error at the surface of the Earth). The error at an altitude of 400 km varies from zero at the poles and equator to less than 13 cm at a latitude of ±45° when compared to the iterative technique of *Hedgley* [1976].

[16] The raypath equations are a set of six coupled first-order ordinary differential equations for the ray position, $\vec{r}$, and the vector $\vec{k}$ which has a magnitude of μ, the refractive index, in the direction of the wave normal. They are solved by numerically integrating them with the embedded fourth/fifth-order eight-step Runge-Kutta algorithm of *Bogacki and Shampine* [1996]. The set of Runge-Kutta parameters (or Butcher table) developed by them yields an efficient algorithm with a high level of accuracy. Adaptive step size control is included and is based on the error estimate obtained from the difference between the fourth- and fifth-order solutions. The solution returned is fourth order.

[17] When the magnetic field is ignored, the independent variable over which the raypath equations are integrated is, conveniently, the group range, P'. However, this is not the case for a magnetized ionosphere. The group range, for this case, must be calculated by integrating the group refractive index, μ', along the ray's path:

$$P' = \int \mu' \cos\alpha \, \mathrm{d}l \tag{1}$$

where α is the angle between the wave normal and ray direction. This angle is easily calculated during the numerical integration:

$$\cos\alpha = \frac{\vec{k} \cdot \dot{\vec{r}}}{\mu \, |\dot{\vec{r}}|} \tag{2}$$

The group refractive index is related to the refractive index as follows:

$$\mu' = \frac{\mathrm{d}(\mu f)}{\mathrm{d}f} \tag{3}$$

where f is the wave frequency of the ray. Multiplying the quadratic form of the Appleton-Hartree equation for μ^2 [see, e.g., *Haselgrove and Haselgrove*, 1960] by f^2, differentiating with respect to f, and after much algebraic manipulation an equation for μ' is derived. This is then solved along with the differential equations for the raypath.

[18] The state vector of the ray, $\vec{S}(\vec{r}, \vec{k})$, is stored at every point along the raypath and output once the numerical integration has completed. Other quantities which are calculated along the raypath and output include the phase path, geometrical distance, refractive index, group refractive index, the angles subtended by the wave normal and ray direction and geomagnetic field, electron density, magnetic field vector, magnitude of the wave polarization, and the tilt angles of the wave electric field vector and volume polarization vector out of the plane of the wavefront.

[19] The various PHaRLAP algorithms are coded in Fortran compliant with the Fortran2008 specification. The routines have been compiled against MathWorks mex libraries to enable them to be called within the MATLAB programming language for ease of use.

[20] Figure 1 shows an example of raypaths for the ordinary (*O*) and extraordinary (*X*) polarization modes calculated using the 3-D magnetoionic ray tracing engine. The green raypath in this figure is the case for no geomagnetic field. The ionosphere used in this example is spherically symmetric; thus, there are no ray deviations due to ionospheric tilts. The deviation of the *O*-mode and *X*-mode rays in this case is due to the magnetic field alone.

[21] In Figure 2 we show the effect of a tilted ionosphere on the raypaths. The ionospheric tilt takes the form of an increase in f_oF2 in a direction perpendicular to the launch azimuth of the rays. We immediately see that the effect of even a small ionospheric tilt is significant and larger than that due to the effect of the geomagnetic field. Figures 1 and 2 clearly demonstrate that in order to model the effects of TIDs, a full 3-D magnetoionic ray tracing procedure is required.

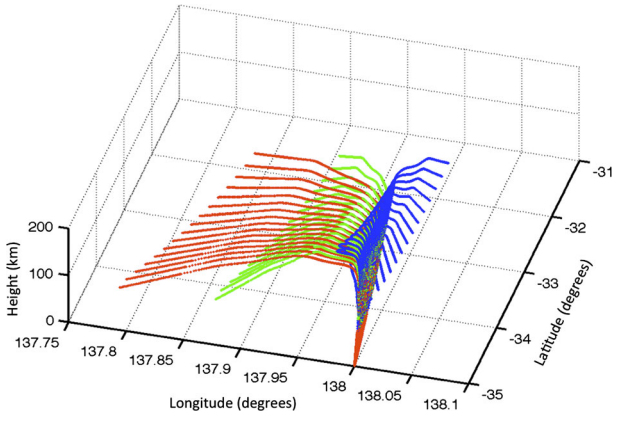

Figure 2. Example of 3-D ray tracing with PHaRLAP showing the effect of a tilted ionosphere. Blue lines are a fan of 5 MHz *O*-mode polarized rays propagated through a spherically symmetric ionosphere. The initial azimuth of these rays is 0°. Note the effect of the geomagnetic field which causes a small out-of-plane deviation. The green lines are initially the same rays as above but propagated through an ionosphere which has a small ionospheric tilt (f_oF2 increase of 0.03 MHz per degree longitude) imposed. The red lines are the rays propagated through an ionosphere which has a larger ionospheric tilt (f_oF2 increase of 0.07 MHz per degree longitude) imposed.

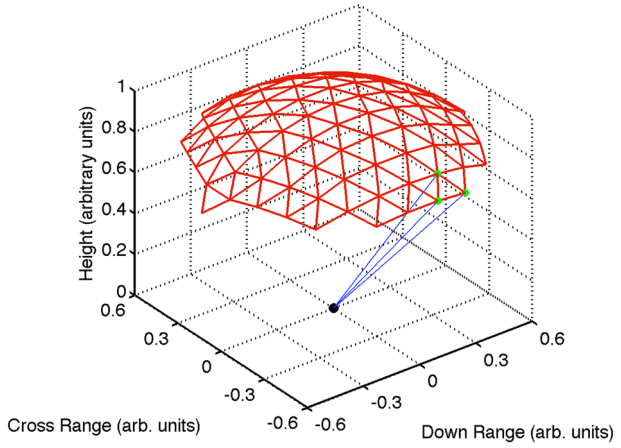

Figure 3. Schematic depicting how the ray launch directions are defined. Each ray from the transmitter (black dot) passes through a triangle vertex. The blue lines indicate three such rays which form a triplet (see text).The triangles are equilateral and identical, ensuring that the ray launch directions are evenly distributed.

3. Synthesis of Disturbed Ionograms

3.1. Overview

[22] The method we use to model ionospheric disturbances is first to model the undisturbed quasi-vertical ionograms (QVI) immediately prior to the presence of a disturbance. This requires the specification of a model ionosphere through which the ray tracing is performed. The model ionosphere is based on quasi-parabolic (QP) layers with the layer parameters tuned such that the model QVI matches the observed undisturbed QVI within some threshold.

[23] Once the undisturbed ionogram has been successfully modeled, we introduce a disturbance. The features of the disturbance are varied until we are able to reproduce the observed features in the disturbed ionogram. This procedure is repeated at various time intervals in order to model the temporal evolution of the ionospheric disturbance as seen in the time sequence of observed ionograms.

3.2. Ionogram Synthesis

[24] We now describe the procedure for modeling an individual ionogram. First, a set of launch vectors are defined that fill a cone from an origin (the transmitter). The vectors are evenly distributed in solid angle with their points of intersection with the surface of a sphere of unit radius centered at the transmitter and taken in triplets defining identical equilateral triangles (see Figure 3). Each of the ray triplets is tagged. Next, rays at a particular frequency are launched along these vectors, and their endpoints on the ground, defined by the ray tracing, are recorded. We then loop over all of the ray triplets and note which of the triplets "surround" the receiver. This is achieved via Delaunay triangulation [see, e.g., *Press et al.*, 2007]. These ray triplets then represent a propagation mode from the transmitter to receiver. The Delaunay triangulation process is also used to interpolate the group range and launch direction of the actual ray which would land at the receiver. This process is repeated at various frequencies and a model ionogram constructed. We use a much greater density of rays than that shown in Figure 3.

[25] The point-to-point ray tracing method of *Coleman* [2011] was not used to synthesize our ionograms. This was due to the requirement for an appropriate initial estimate of the raypath. For the oblique propagation case described by *Coleman* [2011], the out-of-plane deviations due to magnetoionic effects or ionospheric tilts (or TIDs) are small in comparison to the distance the ray has traveled for long raypaths. Thus, a simple technique such as 2-D NRT may be used for the initial estimate of the raypath. However, for the near-vertical case of our experimental setup, determining an initial estimate which adequately represents the raypath is not possible. Near apogee, the wave frequency of the near-vertical rays approaches the critical frequency of the ionosphere (i.e., the refractive index approaches zero). Thus, the rays experience a large deviation in their path with respect to a "simple path" which neglects the effect of the Earth's magnetic field or ionospheric tilts. Furthermore, these deviations are significantly different for the *O* and *X* modes.

3.3. TID Model

[26] Instead of implementing the aforementioned Gaussian troughs and enhancements of *Helms and Thompson* [1973] and *Lobb and Titheridge* [1977] for the TID model, we have decided to employ the theory developed by *Hooke* [1968]. The problem with the Gaussian perturbations is that they have no basis in a causal mechanism. In contrast, the theory developed by *Hooke* is based upon the consideration of atmospheric gravity waves (which are generated in the lower atmosphere) propagating up into the ionosphere. The resultant motions of the neutral gas at these altitudes induce disturbances in the background plasma.

[27] The expression for the perturbation in the background electron density, N_e', derived by *Hooke* is

$$N_e'(\vec{r},t) = |N_e'|e^{(i\psi)} \tag{4}$$

where $\vec{r}$ is position in Cartesian coordinates, t is time, $|N_e'|$ is the magnitude of the perturbation, and ψ is given by

$$\psi = \omega t - \vec{k}\cdot\vec{r} + \tan^{-1}\left[\frac{\sin(I)}{k_{\mathrm{br}}}\left(\frac{1}{N_e}\frac{\partial N_e}{\partial z} + k_{\mathrm{zi}}\right)\right] \tag{5}$$

Here $\vec{k}$ and ω are the phase vector and angular frequency of the perturbing gravity wave, I is the inclination of the geomagnetic field, k_{zi} is the imaginary part of the vertical component of phase propagation vector, and k_{br} is the real part of the component of the phase propagation vector parallel to the magnetic field. In the absence of dissipation, $k_{\mathrm{zi}} = 1/2H$, where H is the scale height. The $\omega t - \vec{k}\cdot\vec{r}$ term is the standard expression for wave propagation while the remaining term is an additional height-varying phase term. The magnitude of the electron density perturbation is given by

$$|N_e'| = N_e U_b(z_0) e^{[k_{\mathrm{zi}}(z-z_0)]}\omega^{-1}\sin(I)\cdot\left[\left(\frac{1}{N_e}\frac{\partial N_e}{\partial z}\right) + \left(\frac{k_{\mathrm{br}}}{\sin(I)}\right)^2\right]^{1/2}, \tag{6}$$

where N_e is the unperturbed electron density and $U_b(z_0)$ the magnitude of the neutral gas velocity parallel to the magnetic field at reference height z_0. The exponential term in

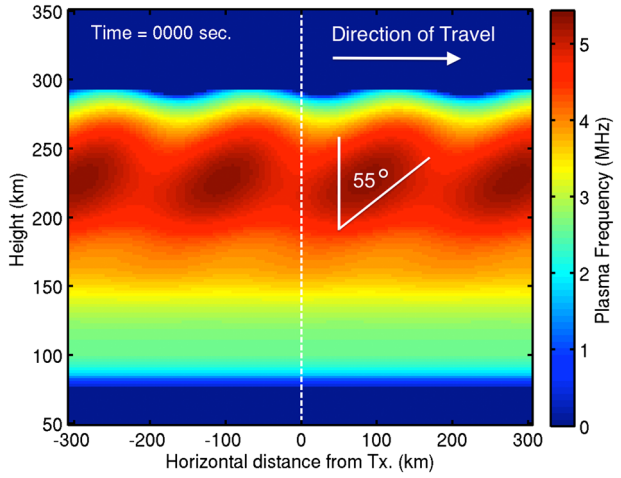

Figure 4. Example of a model ionospheric disturbance produced by a gravity wave with a period of 20 min, horizontal wavelength of 200 km, and U_b of 15 ms^{-1}. The TID is phase advanced with height (i.e., tilted) in the direction of travel with a tilt angle of 55°. The model TID is invariant in cross-range.

this expression drives growth of the ionospheric disturbance with altitude and is due to the growth of the gravity wave amplitude with decreasing neutral gas density. This is counteracted by the dissipation term in the large square brackets which is due to the effect of molecular dissipation on gravity waves in the upper atmosphere [*Hines*, 1968].

[28] These expressions are valid only for the bottom side of the F layer. Above the F layer peak, the processes become nonlinear due to the rapidly decreasing atmospheric densities (both neutral and ionic). The gravity waves break, and the behavior and interaction with the ionosphere are complex and must be described by a set of partial differential equations. This is not required for our purposes. A similar treatment for the E layer yields expressions for the electron density perturbations in this layer [*Hooke*, 1969]. However, in this paper we restrict ourselves to TIDs in the F layer.

[29] We make the assumption that the phase fronts of the gravity waves are planar and choose our coordinate frame such that the direction of travel is parallel to one of the horizontal axes. Thus, $\vec{k} = (k, 0, m)$, where k and m are the horizontal and vertical wave numbers and are related by the dispersion relation for gravity waves:

$$m^2 = k^2 \left(\frac{\omega_B^2}{\omega^2} - 1 \right) + \frac{(\omega^2 - \omega_a^2)}{c^2} \tag{7}$$

where ω_B is the Brunt-Väisälä frequency, ω_a is the acoustic cutoff frequency, and c is the speed of sound. For gravity waves, $\omega < \omega_a$. These parameters are determined by the neutral atmospheric conditions:

$$\omega_B = \frac{(\gamma - 1)g}{\gamma H}, \quad c = \sqrt{\gamma g H}, \quad \omega_a = \frac{c}{2H} \tag{8}$$

where g is acceleration due to gravity, γ is the ratio of the specific heat of dry air at constant pressure to the specific heat at constant volume, and H is the scale height which varies with altitude. The scale height is defined by

$$H = \frac{k_B T}{\bar{\mu} m_u g} \tag{9}$$

where k_B is Boltzmann's constant, T is temperature, $\bar{\mu}$ is the mean molecular mass of the atmospheric constituents, and m_u is the atomic mass unit. We use the NRLMSISE-00 model of the neutral atmosphere [*Picone et al.*, 2002] to specify T and $\bar{\mu}$.

[30] Figure 4 displays an example of a TID generated by a gravity wave in the Adelaide region, traveling in the direction 225° from north. We set the horizontal wavelength of the perturbing gravity wave to be 200 km, the period at 20 min, and U_b to be 15 ms^{-1} at a reference height of 250 km. The resultant TID is tilted forward at an angle of ~ 55°, while the vertical wavelength and the horizontal component of the group velocity may be determined from the dispersion relation and have values of 140 km and 112 ms^{-1}.

4. Results

4.1. Undisturbed Ionogram

[31] Figure 5 shows an ionogram recorded at 22:07 UT on 26 February 2008 (27 February 07:37 LT) during the first SpICE campaign [*Harris et al.*, 2012]. The transmitter was located at Woodside, South Australia in the Adelaide hills, and the receiver at DSTO Edinburgh ~ 40 km away. Superposed on the ionogram are black dots and crosses indicating the modeled ionogram for the O and X polarization modes. The plasma frequency profile of the model ionosphere we used to generate the model ionogram is the blue curve in this figure and is produced from Quasi-Parabolic (QP) layers. The layer parameters describing this profile are f_oE = 2.61 MHz, h_mE = 105.0 km, y_mE = 25.0 km, f_oF1 = 4.0 MHz, h_mF1 = 180.0 km, y_mF1 = 65.0 km, f_oF2 = 5.1 MHz, h_mF2 = 224.0 km, and y_mF2 = 68.0 km. An inverse

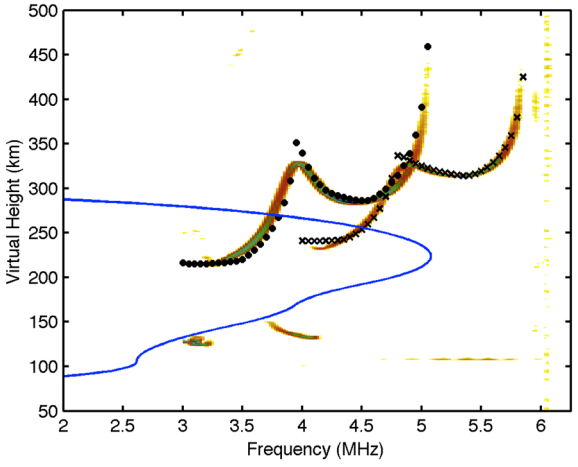

Figure 5. Quasi-vertical ionogram observed at 22:07 UT on 26 February 2008 immediately prior to the passage of an ionospheric disturbance with superposed modeled ionogram (O-mode, black dots; X-mode, black crosses). The blue curve is the plasma frequency profile of the model ionosphere used to generate this undisturbed model ionogram. The QP layer parameters are listed in the text.

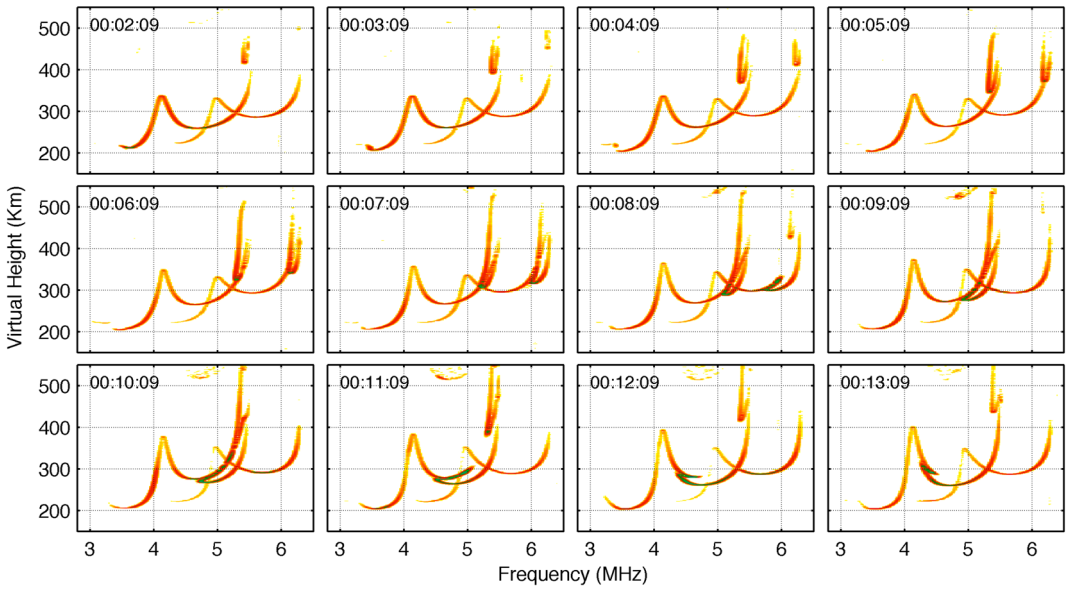

Figure 6. A series of quasi-vertical ionograms observed on 27 February 2008 displaying the passage of a TID. Time stamps are UT, and the dynamic range of the images is 30 dB.

parabolic profile is used to join the E and F1 layers. While the agreement between the observed and model ionograms is generally good, there are some minor differences. This is due to the parameterized model ionosphere not having enough degrees of freedom to fully describe the real ionosphere. In subsequent work, we intend to use the POLynomial ANalysis (POLAN) program [*Titheridge*, 1985] to invert the observed ionograms to obtain an ionospheric profile which more accurately represents the real ionosphere than the QP parametric model.

4.2. TID Event 22:10 UT, 26 February 2008

[32] Figure 6 displays a series of ionograms recorded at DSTO Edinburgh (transmitter at Woodside) at 1 min intervals. These ionograms indicate the passage of a TID, and its manifestation is typical of the type of disturbance features we observe in our data (see *Harris et al.* [2012] for a detailed discussion). This particular disturbance feature is one of several in a train occurring with a period of ∼20 min and was discussed in our earlier paper [*Harris et al.*, 2012]. In that paper we were not sure what the mechanism was which generated a disturbance feature which progressed down the "inside" (i.e., at a lower frequency) of the main trace. We shall see later in this section that gravity waves are not only eminently plausible but most likely the causal mechanism.

[33] We have attempted to model this disturbance feature as being caused by a gravity wave with a horizontal wavelength of 175 km, period of 20 min, and U_b of 10 ms^{-1} at a reference height of 250 km. This results in a vertical wavelength of 122 km and horizontal group speed of 98 ms^{-1} (the horizontal phase speed is 146 ms^{-1}). The direction of travel of the gravity wave is 225° from north. The horizontal speed is typical of small-scale TIDs [*Hocke and Schlegel*, 1996] while the value of U_b corresponds to the magnitude of the neutral gas velocity (due to the gravity wave) being ∼ 37 ms^{-1}.

[34] Due to invariance of the TID in cross-range, we are able to reduce the number of rays we need to trace to synthesize the ionogram and thus speed up the process. Once an ionogram has been synthesized, time is incremented, the ionosphere updated with the disturbance having traveled the appropriate distance, and a new ionogram synthesized. In this manner we are able to build a movie of the modeled disturbed ionogram. A total of 50 time steps are used for the passage of one wavelength of the TID. This corresponds to a time resolution of 24 s in our movies.

[35] Figure 7 displays a series of snapshots of the synthesized TID movie (see supporting information). In general, we see that the synthesized ionograms capture the behavior of the observed TID and we make the following statements:

[36] 1. In both observed and modeled ionograms, the disturbance on the *O*-mode appears earlier than that on the *X*-mode. They appear as "U-shaped" features with the observed features narrower than modeled. As time progresses, the disturbance on the *X*-mode of both observed and modeled ionograms "catches up" to the *O*-mode disturbance.

[37] 2. At 00:03:09 (Figure 6, panel 2) the observed minimum virtual height of the *O*-mode disturbance is 390 km and for the *X*-mode 450 km; a difference of 60 km. Three minutes later at 00:06:09 (Figure 6, panel 5), the observed difference has reduced to 15 km. Similar behavior is noted in the modeled ionogram: at 00:00:48 (Figure 7, panel 3), the difference between the *O*-mode and *X*-mode virtual height is 45 km which reduces to 18 km after 3 min.

[38] 3. As time progresses, the disturbance feature moves down the inside of the main trace in both the observed and modeled ionograms and then "crosses over" to the outside of the main trace. A prominent disturbance feature is imposed upon the main trace which evolves and appears progressively at lower frequencies while the original disturbance feature recedes back up inside the main trace.

[39] 4. The *X*-mode disturbance (higher frequency trace) "crosses over" the main trace before the *O*-mode in both observed and model ionograms. It starts to recede some time between 00:07:09 and 00:08:09 (Figure 6, panels 6–7) for the observed ionograms (∼5 min after the disturbance is first observed) and between 00:04:24 and 00:04:48 (Figure 7,

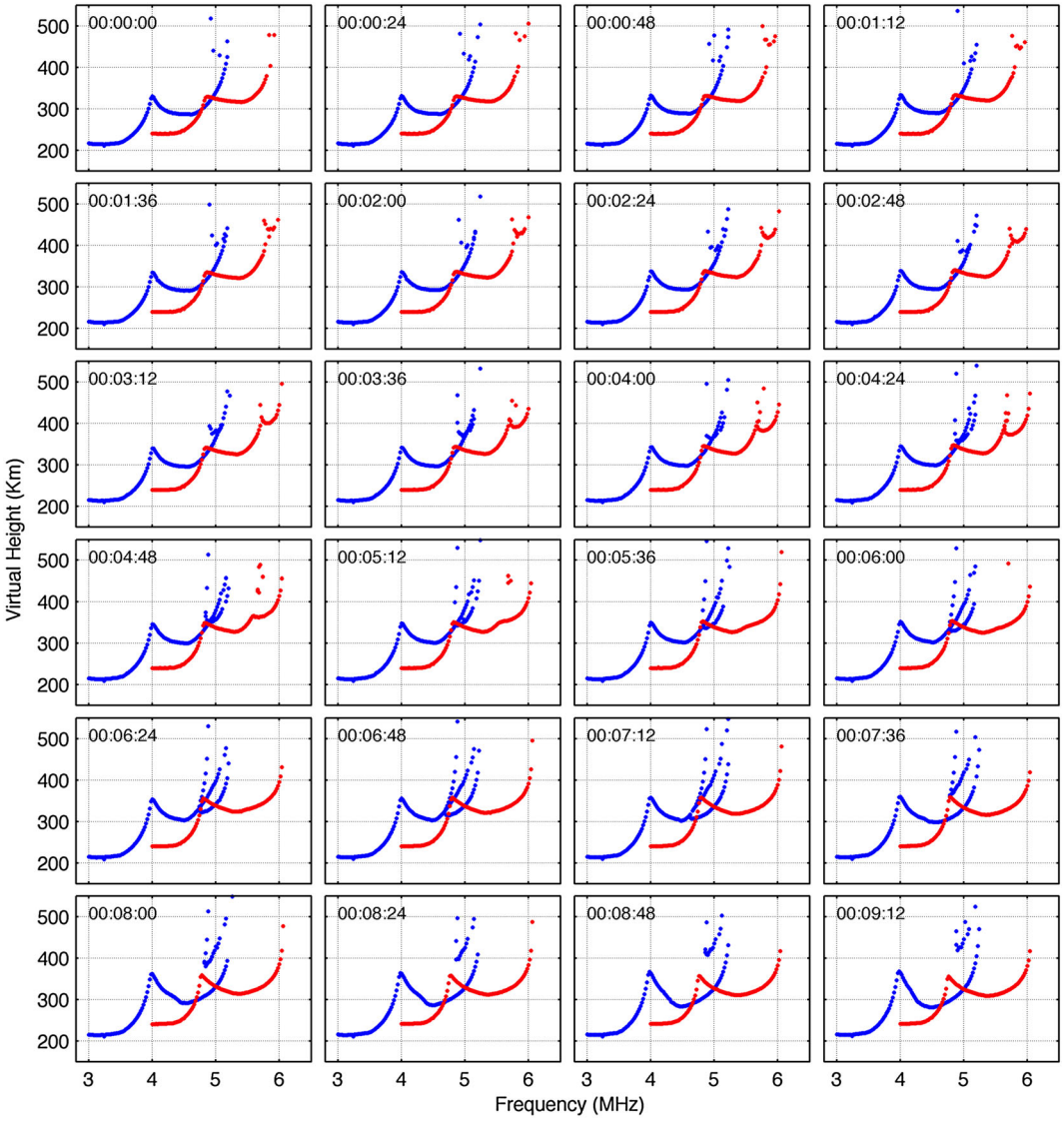

Figure 7. A synthesized series of quasi-vertical ionograms displaying the passage of a TID generated by a gravity wave (see text for details).

panels 12–13) with the modeled ionograms (∼4.5 min after the disturbance is first noted in the model).

[40] 5. The signature imposed on the observed *X*-mode main trace and the original feature, which now moves back up inside the main trace, disappears rapidly (unlike the *O*-mode) and this is the case for both the modeled and observed ionograms. The observed prominent main trace disturbance signature (see Figure 6, panel 7 at 00:08:09) is not so evident in the model ionogram. However, an inflection or kink in the modeled *X*-mode main trace is noted at the point where the signature would be expected to occur (see Figure 7, panel 13 at 00:04:48).

[41] 6. At ∼ 7.5 min after the disturbance has been initially observed, the *O*-mode disturbance displays similar behavior to that noted on the *X*-mode earlier in point 5 above. The modeled *O*-mode disturbance behavior is similar to that observed and also occurs at ∼ 7.5 min.

[42] 7. The signature which develops on the observed *O*-mode main trace at ∼ 7.5 min is similar to but more prominent than that observed on the *X*-mode earlier. It lasts much longer than that on the *X*-mode and appears progressively at lower frequencies. As with the *X*-mode, the modeled ionograms do not display this obvious signature but rather an inflection is noted in the modeled main trace which also moves to lower frequencies as time progresses.

[43] 8. As noted on the *X*-mode in point 5 above, the original disturbance feature recedes back up inside the main trace. However, for the *O*-mode case (both observed and modeled), this signature is much more prominent than that for the *X*-mode and is present for longer before it disappears.

[44] It is evident that most of the major features of the disturbance observed in the ionograms and its evolution are captured by the model. This suggests that the theory developed by *Hooke* [1968] (i.e., gravity waves perturbing the ionosphere) is a plausible mechanism for the generation of TIDs.

[45] The modulation of the reflection points of the radio waves by the TID is a complicated process. PHaRLAP can be used to visualize this modulation, allowing the relationship between the appearance of the QVI disturbance features

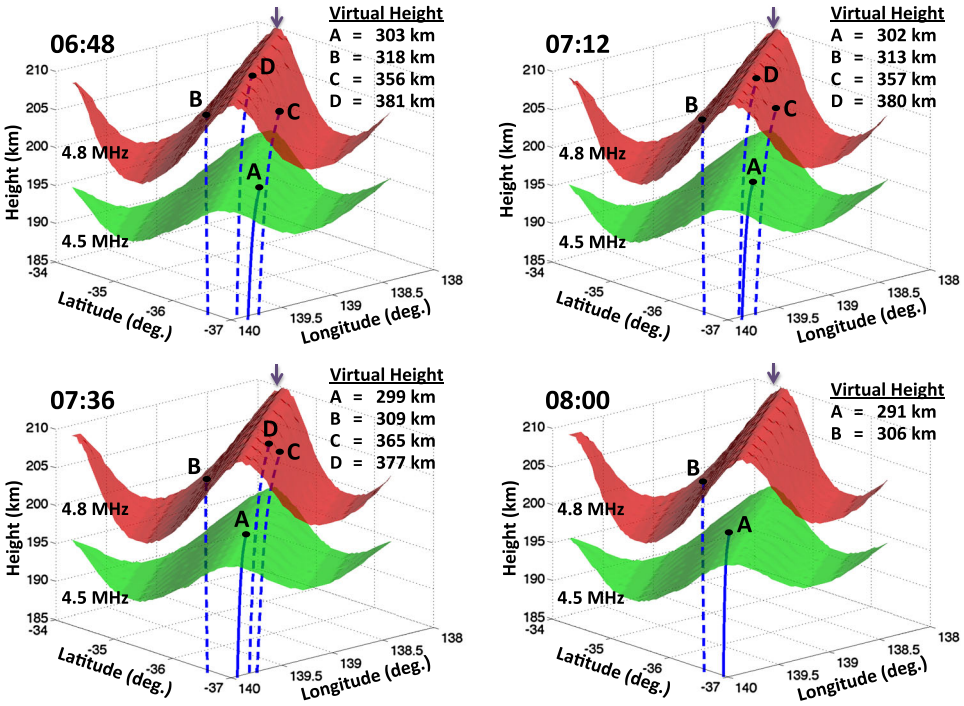

Figure 8. Isoionic surfaces of the ionosphere perturbed by the gravity wave from Figure 7 at four successive times (indicated at the top left of each plot in minutes and seconds). The green isoionic surface is at a plasma frequency of 4.5 MHz and the red surface is at 4.8 MHz. The blue lines are rays representing QVI propagation modes at 4.5 MHz (solid) and 4.8 MHz (dashed). For clarity, only the up-leg of the rays are shown. Black dots indicate the reflection points of the rays and their virtual heights are noted in the tables (top right of each plot). The purple arrow at the top of each plot is in the same location for each case and is a visual aid to indicate the motion of the TID from one time step to the next.

and the modulation of the reflection points to be better understood. This is shown in Figure 8 where the reflection points of rays representing QVI propagation modes at two frequencies (4.5 and 4.8 MHz) are modulated by the passage of the TID. At each of the four time instances displayed, only one propagation mode (ray A) exists at 4.5 MHz. This mode forms the main trace of the ionogram at 4.5 MHz. However, at 4.8 MHz three modes (rays B, C, and D) exist at the first 3 time steps with only one remaining (ray B) at the last time step. Ray B forms the main trace of the ionogram at 4.8 MHz, while rays C and D form the disturbance feature which recedes up inside the main trace as time progresses. Note the motion of the reflection points of rays C and D toward coincidence as time progresses and the consequential narrowing of their virtual height difference. This explains the shape of the receding disturbance feature in the ionograms. Once the TID has moved sufficiently (fourth plot at 08:00 min), only one propagation mode remains at 4.8 MHz and so the disturbance feature in the ionogram disappears at this frequency.

[46] Figure 8 also explains why, unlike the observations, a strong disturbance feature is not produced on the main trace of the modeled ionograms at the lower frequencies which then moves down the main trace as time progresses.

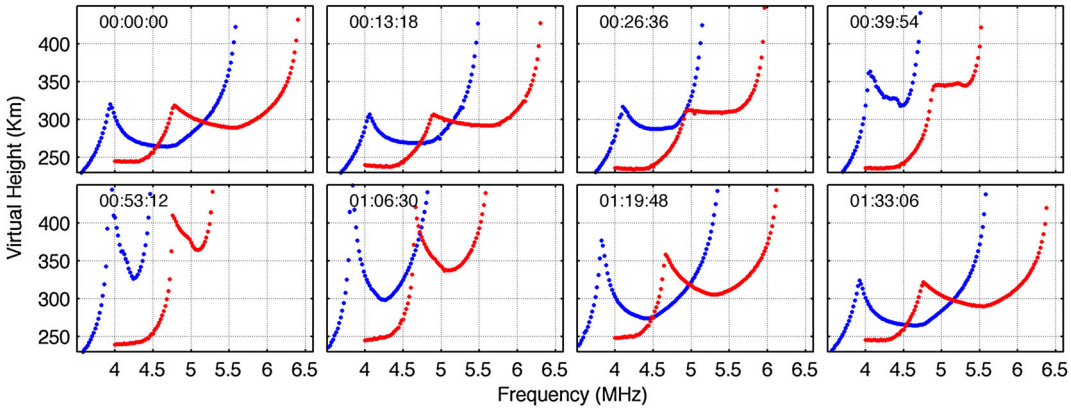

Figure 9. A synthesized series of quasi-vertical ionograms displaying the passage of a medium- to large-scale TID generated by a gravity wave (see text for details).

The electron density gradient of the 4.5 MHz isoionic surface is much less than that at 4.8 MHz, and consequently, only one propagation mode is supported. This indicates that the gravity wave theory of *Hooke* [1968] does not produce a strong enough disturbance in the ionosphere at the lower altitudes where the ionosphere is weaker. Modification of the k_{zi} parameter, which controls the dissipation of the gravity wave, may be necessary. However, that investigation is beyond the scope of this paper.

[47] The final point we make in this discussion is that the TIDs were also modeled using the Gaussian troughs and enhancements of *Lobb and Titheridge* [1977]. The reason for doing this was so we could vary the forward tilt of the isoionic contours. We found that we could replicate the form of the observed disturbances when a forward tilt angle was chosen to match that of the gravity waves ($\sim 55°$ in our case). However, when different tilt angles were chosen, we could not replicate the observations. This strengthens the argument that gravity waves are the mechanism which generated this TID.

4.3. Medium- to Large-Scale TIDs

[48] In our previous paper [*Harris et al.*, 2012] we found that variations in the ionospheric parameter h'F2 was a good indicator of TID activity. By examining the cross-correlation function of appropriately band-passed data at each of the ionospheric probe points, we were able to deduce that a medium- to large-scale TID was present. Assuming that this TID was due to wave activity, we obtained a phase speed of 305 ms^{-1} at a bearing of 293°. A power spectral analysis indicated that the period of the wave activity was $\sim$ 95 min from which we obtain a wavelength of $\sim$ 1700 km.

[49] It was clear from our power spectral analysis that TIDs at several different scale sizes were present simultaneously in our data. It was also evident that the ionograms respond differently to TIDs of different scale sizes. This is also apparent with the model ionograms. In Figure 9 we display the time sequence of model ionograms where the ionosphere has been perturbed by a large-scale TID with the parameters above. We see that the model ionograms respond with h'F2 rising and falling as observed by *Harris et al.* [2012]. The additional cusps or loops are not evident at all.

[50] Figure 10 displays the variation of h'F2 and f_oF2 data scaled from QVI ionograms observed on 27 February 2008 over the Woodside to DSTO Edinburgh path [see *Harris et al.*, 2012, for details]. The effect of the large-scale TID is clearly discerned. Also displayed in this figure are the modeled h'F2 and f_oF2 variation. We note that the modeled h'F2 variation agrees well with that observed. However, while the modeled f_oF2 variation is similar to that observed, it is significantly larger than the observed f_oF2 early in the time series. A similar but much smaller discrepancy is also noted in the h'F2 comparison. We believe that this is due to the background f_oF2 increasing with time due to the solar zenith angle effect (the data were collected just after sunrise), whereas we did not account for this effect in the modeling; a constant ionospheric background was used. It is beyond the scope of this paper to account for this effect. Not withstanding the increase in strength of the background ionosphere affecting the f_oF2 variation, Figure 10 is consistent with the hypothesis that the long period variations

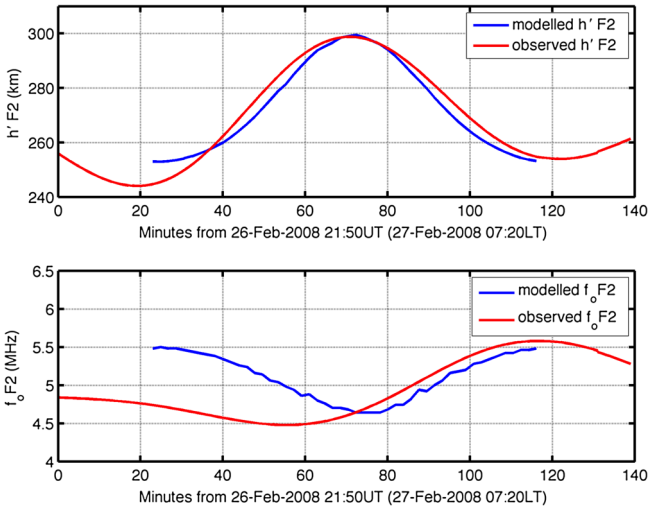

Figure 10. Modeled and observed (top) h'F2 and (bottom) f_oF2 variation due to the passage of a medium- to large-scale TID (see text for details).

observed in our QVI ionograms were due to a medium- to large-scale TID generated by gravity wave activity in the neutral atmosphere.

5. Concluding Remarks and Future Work

[51] We have shown that Hamiltonian ray tracing techniques may be used to model disturbance features observed in quasi-vertical ionograms and thus allow us to gain insight into the form of the disturbances in the ionosphere. The disturbances that we have modeled in this paper include both small- and large-scale TIDs and are typical of what we observe in our data. These TIDs were relatively simple to model and were consistent with being produced by gravity wave activity in the neutral atmosphere perturbing the ionosphere.

[52] We have observed many other less common disturbances which are more difficult to interpret. Modeling these disturbances will be the subject of future work. This will require an analysis of how modifying the gravity wave parameters (e.g., wavelength, strength, and direction of travel with respect to the direction of the geomagnetic field) affects how the disturbance features are manifest in the modeled ionograms.

[53] **Acknowledgments.** The authors would like to acknowledge helpful discussions with Dan Meehan and Ken Lynn. The ray tracing results presented in this paper were produced by the raytracing toolbox PHaRLAP. This toolbox is available by request from its author, Manuel Cervera.

[54] Robert Lysak thanks Dave Neudegg and an anonymous reviewer for their assistance in evaluating this paper.

References

Bennett, J. A. (1969), On the application of variation techniques to the ray theory of radio propagation, *Radio Sci.*, *4*, 667–678, doi:10.1029/RS004i008p00667.

Bennett, J. A. (1973), Variations of the ray path and phase path: A Hamiltonian formulation, *Radio Sci.*, *8*, 737–744, doi:10.1029/RS008i008p00737.

Bennett, J. A., P. L. Dyson, and R. N. Norman (2004), Progress in radio ray tracing in the ionosphere, *Radio Sci. Bull.*, *310*, 81–91.

Bogacki, P., and L. F. Shampine (1996), An efficient Runge–Kutta (4,5) pair, *Comput. Math. Appl.*, *32*(6), 15–28.

Booker, H. G. (1961), A local reduction of F-region ionization due to missile transit, *J. Geophys. Res.*, *66*, 1073–1079, doi:10.1029/JZ066i004p01073.

Coleman, C. J. (1997), On the simulation of backscatter ionograms, *J. Atmos. Sol. Terr. Phys.*, *59*, 2089–2099, doi:10.1016/S1364-6826(97)00038-2.

Coleman, C. J. (1998), A ray tracing formulation and its application to some problems in over-the-horizon radar, *Radio Sci.*, *33*, 1187–1198, doi:10.1029/98RS01523.

Coleman, C. J. (2011), Point-to-point ionospheric ray tracing by a direct variational method, *Radio Sci.*, *46*, RS5016, doi:10.1029/2011RS004748.

Croft, T. A. (1967), Computation of HF ground backscatter amplitude, *Radio Sci.*, *2*, 739–746.

Croft, T. A., and H. Hoogasian (1968), Exact ray calculations in a quasi-parabolic ionosphere with no magnetic field, *Radio Sci.*, *3*, 69–79.

Dyson, P. L., and J. A. Bennett (1988), A model of the vertical distribution of the electron concentration in the ionosphere and its application to oblique propagation studies, *J. Atmos. Terr. Phys.*, *50*, 251–262.

EL-Rabbany, A. (2006), *Introduction to GPS: The Global Positioning System*, Artech House, Boston, Mass.

Harris, T. J., M. A. Cervera, and D. H. Meehan (2012), SpICE: A program to study small-scale disturbances in the ionosphere, *J. Geophys. Res.*, *117*, A06321, doi:10.1029/2011JA017438.

Haselgrove, C. B., and J. Haselgrove (1960), Twisted ray paths in the ionosphere, *Proc. Phys. Soc. London*, *75*, 357–363.

Haselgrove, J. (1955), Ray theory and a new method for raytracing, in *Physics of the Ionosphere*, pp. 355–364, Physical Society, London.

Haselgrove, J. (1963), The Hamiltonian ray path equations, *J. Atmos. Terr. Phys.*, *25*, 397–399.

Hedgley, D. R. (1976), An exact transformation from geocentric to geodetic coordinates for nonzero altitudes, *NASA Technical Report, TR R-458*.

Helms, W. J., and A. D. Thompson (1973), Ray-tracing simulation of ionization trough effects upon radio waves, *Radio Sci.*, *8*, 1125–1132, doi:10.1029/RS008i012p01125.

Hines, C. O. (1968), An effect of molecular dissipation in upper atmospheric gravity waves, *J. Atmos. Terr. Phys.*, *30*, 845–849, doi:10.1016/S0021-9169(68)80036-4.

Hocke, K., and K. Schlegel (1996), A review of atmospheric gravity waves and traveling ionospheric disturbances: 1982–1995, *Ann. Geophys.*, *14*, 917–940.

Hooke, W. H. (1968), Ionospheric irregularities produced by internal atmospheric gravity waves, *J. Atmos. Terr. Phys.*, *30*, 795–823, doi:10.1016/S0021-9169(68)80033-9.

Hooke, W. H. (1969), E-region ionospheric irregularities produced by internal atmospheric gravity waves, *Planet. Space Sci.*, *17*, 749–765, doi:10.1016/0032-0633(69)90195-0.

Jones, R. M. (1968), A three-dimensional ray tracing computer program, *Radio Sci.*, *3*, 93–94.

Jones, R. M., and J. J. Stephenson (1975), A versatile three-dimensional ray tracing computer program for radio waves in the ionosphere, *NASA STI/Recon Technical Report N, 76*, 25,476.

Kalikhman, A. D., N. N. Klimov, G. K. Matafonov, and A. V. Tashchilin (1992), Simulation of ionosonde observations of ionospheric holes, *J. Atmos. Terr. Phys.*, *54*, 1177–1179.

Lobb, R. J., and J. E. Titheridge (1977), The effects of travelling ionospheric disturbances on ionograms, *J. Atmos. Terr. Phys.*, *39*, 129–138.

Mathworks (2013), Geocentric to Geodetic Latitude. http://www.mathworks.com/access/helpdesk/help/toolbox/aeroblks/geocentrictogeodeticlatitude.html, The Mathworks Inc., Natick, MA 01760-2098, USA.

Munro, G. H. (1953), Reflexions from irregularities in the ionosphere, *Proc. R. Soc. London A*, *219*, 447–463.

Munro, G. H., and L. H. Heisler (1956a), Cusp type anomalies in variable frequency ionospheric records, *Aust. J. Phys.*, *9*, 343–358, doi:10.1071/PH560343.

Munro, G. H., and L. H. Heisler (1956b), Divergence of radio rays in the ionosphere, *Aust. J. Phys.*, *9*, 359–372, doi:10.1071/PH560359.

Nickisch, L. J. (1988), Focusing in the stationary phase approximation, *Radio Sci.*, *23*, 171–182, doi:10.1029/RS023i002p00171.

Norman, R. J., P. L. Dyson, and J. A. Bennett (1997), Analytic ray parameters for the quasi-cubic segment model of the ionosphere, *Radio Sci.*, *32*, 567–578, doi:10.1029/96RS03521.

Paul, A. K., G. H. Smith, and J. W. Wright (1968), Ray-tracing synthesis of ionogram observations of a large local disturbance in the ionosphere, *Radio Sci.*, *3*, 15–26.

Picone, J. M., A. E. Hedin, D. P. Drob, and A. C. Aikin (2002), NRLMSISE-00 empirical model of the atmosphere: Statistical comparisons and scientific issues, *J. Geophys. Res.*, *107*(A12), 1468, doi:10.1029/2002JA009430.

Press, W. H., S. A. Teukolsky, W. T. Vetterling, and B. P. Flannery (2007), *Numerical Recipes: The Art of Scientific Computing*, Cambridge Univ. Press, Cambridge, U. K.

Reilly, M. H. (1991), Upgrades for efficient three-dimensional ionospheric ray tracing: Investigation of HF near vertical incidence sky wave effects, *Radio Sci.*, *26*, 971–980, doi:10.1029/91RS00582.

Russell, C. J., P. L. Dyson, Z. Houminer, J. A. Bennett, and L. Li (1997), The effect of large-scale ionospheric gradients on backscatter ionograms, *Radio Sci.*, *32*, 1881–1898, doi:10.1029/97RS01397.

Stocker, A. J., N. F. Arnold, and T. B. Jones (2000), The synthesis of travelling ionospheric disturbance (TID) signatures in HF radar observations using ray tracing, *Ann. Geophys.*, *18*, 56–64, doi:10.1007/s00585-000-0056-4.

Strangeways, H. J. (2000), Effect of horizontal gradients on ionospherically reflected or transionospheric paths using a precise homing-in method, *J. Atmos. Sol. Terr. Phys.*, *62*, 1361–1376, doi:10.1016/S1364-6826(00)00150-4.

Surtees, W. J. (1968a), A ray-tracing study of direction-of-arrival variations through a traveling ionospheric disturbance, in *Acoustic-Gravity Waves in the Atmosphere*, edited by T. M. Georges, p. 411, US Government Printing Office, Washington, D.C.

Surtees, W. J. (1968b), An approximate synthesis of HF backscatter considering ionospheric motions, *Radio Sci.*, *3*, 57–67.

Titheridge (1985), Ionogram analysis with the generalised program POLAN, *Tech. Rep. UAG-93*, World Data Center A for Solar-Terrestrial Physics.

Tsai, L.-C., C. H. Liu, and J. Y. Huang (2010), Three-dimensional numerical ray tracing on a phenomenological ionospheric model, *Radio Sci.*, *45*, RS5017, doi:10.1029/2010RS004359.

Västberg, A., and B. Lundborg (1996), Signal intensity in the geometrical optics approximation for the magnetized ionosphere, *Radio Sci.*, *31*, 1579–1588, doi:10.1029/96RS02630.